ELSEVIER

Physica B 318 (2002) 341–349

PHYSICA B

www.elsevier.com/locate/physb

Inelastic X-ray scattering and the high-frequency dynamics of disordered systems

T. Scopigno[a,*], U. Balucani[b], G. Ruocco[a], F. Sette[c]

[a] *Dipartimento di Fisica and INFM, Universitá di Roma "La Sapienza", I-00185 Roma, Italy*
[b] *Instituto di Elettronica Quantistica CNR, I-50127 Firenze, Italy*
[c] *European Synchrotron Radiation Facility, B.P. 220 F-38043, Grenoble Cedex, France*

Abstract

Inelastic X-ray scattering (IXS) is a novel spectroscopic technique that recently came up in addition to inelastic neutron scattering (INS), allowing one a determination of the microscopic dynamics in the Thz frequency region and over lengthscales comparable to the mean interparticle separations. The experimental basis of this method will be illustrated, along with a recent selection of examples on its application to the study of the high-frequency collective modes in liquids and glasses, emphasizing the relative merits and drawbacks with respect of INS. In particular, it will be shown how on the snapshot timescale accessed by IXS both the dynamics of the glassy and of the liquid state exhibit similar features and can be described within the same formalism.

Keywords: Collective modes; Dynamics of relaxation phenomena; X-ray scattering; Vibrational states in disordered systems

1. Introduction

The investigation of the collective dynamics in disordered systems constitutes a very active field of research since the beginning of modern science. The absence of translational invariance, indeed, is at the origin of many macroscopic properties which differentiate this state of matter from the crystalline phases. These properties have stimulated many efforts, both theoretical and experimental, to characterise the dynamical and structural properties in the widest possible region of time- and length-scales.

A key-quantity, from both theoretical and experimental points of view, for the determination of the collective dynamics associated with density fluctuations is the dynamical structure factor, $S(Q,E)$. It is defined as the Fourier transform in space and time of the particles' density pair correlation function, and exhibits features in both the energy E and the wavevector Q which correspond to the characteristic excitations of the system:

$$S(Q,E) = \frac{1}{2\pi}\frac{1}{N}\int \mathrm{d}t\, \mathrm{e}^{\mathrm{i}\omega t} \sum_{m,n} \langle \mathrm{e}^{\mathrm{i}\mathbf{Q}\cdot\mathbf{r}_m(t)}\, \mathrm{e}^{-\mathrm{i}\mathbf{Q}\cdot\mathbf{r}_n(0)} \rangle \tag{1}$$

with N being the number of particles in the system whose positions at time t are $\mathbf{r}_n(t)$ $(n = 1, \ldots, N)$. From the theoretical point of view, one can derive the general expression of $S(Q,E)$ in two limiting cases, corresponding, respectively, to either $Q \to 0$ or $Q \to \infty$. In the first case, one considers the

*Corresponding author.
E-mail address: tullio.scopigno@phys.uniromal.it (T. Scopigno).

0921-4526/02/$ - see front matter
PII: S0921-4526(02)00803-7

medium as a continuum and the excitations on such a long time scale that the system can be assumed to be in thermodynamical equilibrium. Under such approximations, one builds up the hydrodynamic theory from the equations of conservation of energy, momentum and number of particles. This allows to derive an explicit expression for $S(Q,E)$ [1]. The spectrum comprises three lines, referred to as the Brillouin triplet, which are centred at $E=0$ and $E=\pm\hbar c_0 Q$, and correspond, respectively, to the entropy fluctuations, and to the compression wave propagating with the adiabatic sound velocity C_0. The two lines at $E=\pm\hbar c_0 Q$ correspond to the energy loss and energy gain and have a width $(D_V+(\gamma-1)D_T)Q^2$ controlled by the longitudinal kinematic viscosity D_V, the thermal diffusion coefficient D_T, and the specific heat ratio γ. The width of the line centred at $E=0$ is proportional to $D_T Q^2$. In the opposite limit of $Q\to\infty$, one assumes the validity of the impulse approximation, where the final state of the excited particle has a kinetic energy much higher than the potential energy, and the wavefunction is therefore well represented by a plane wave. Under these conditions, the $S(Q,E)$ lineshape reflects the initial state momentum distribution, i.e., in a classical fluid, the Boltzmann distribution. The $S(Q,E)$ reduces to a Gaussian centred at the recoil energy $\hbar^2Q^2/2M$, with standard deviation $\sigma=\hbar Q\sqrt{K_B T/M}$, where M is the particle mass. In this limit, the dynamics becomes that of free-particles between successive collisions. These two extreme limits, reflecting idealised situations, neglect the details of the interactions among particles and their effects on the dynamics. On the other hand, the understanding of these interactions constitute the main motivation of modern studies on the dynamics of fluids and disordered systems in general.

The investigation of the collective dynamics in disordered systems beyond the hydrodynamic and single-particle limits outlined above, becomes of particular interest when one considers an intermediate time- and length-scale; namely, more specifically, when one considers distances comparable to those that characterise structural correlations among particles, and times comparable to the lifetime of these correlations. In this intermediate scale, one expects to observe a large modification of the dynamics when the considered times are either much larger or much shorter than those associated to the relaxation of a spontaneous density fluctuation into its equilibrium state.

The dynamics in this intermediate region is studied, theoretically, attempting to extend the hydrodynamic theory to small distances and short times; numerically, employing simulation methods based on the integration of the equations of motion of an ensemble of particles interacting through a specific model potential; and, experimentally, using scattering methods to determine directly the dynamic structure factor.

Quite generally, as far as one considers Q-transfers that are small with respect to $Q_m\approx 2\pi/d$, where d is the mean interparticles distance and Q_m is the Q-value corresponding to the first maximum in the static structure factor $S(Q)$, one finds that $S(Q,E)$ preserves a three-modes lineshape as in the hydrodynamic limit. This behaviour is predicted by both generalised hydrodynamics and molecular hydrodynamic theories, obtained by the assumption of a Q and E dependence of the parameters entering into the constitutive equations. Technically, this is accomplished by the introduction of the memory function formalism, which allows to evidentiate the coupling between the density fluctuations and the relaxation processes active in the system. The continuous evolution from the Brillouin triplet in the hydrodynamic limit towards a more complex three-peaks structure has been found by a large number of molecular dynamics (MD) simulations. For example, in the case of simple monoatomic fluids, this evolution has been confirmed by several MD studies performed with both hard spheres [2] and Lennard–Jones potentials [3]. Experimentally, using Brillouin light scattering (BLS) spectroscopy, one can study $S(Q,E)$ up to Q-values of the order of $0.04\,\mathrm{nm}^{-1}$, i.e., well within the expected range of validity of the hydrodynamic theory. However, even in this small Q range, one needs to introduce energy-dependent transport coefficients associated with the presence of a relaxation process having a characteristic time τ in the *nano*-second range. This need manifests itself by the modifications of the Brillouin line width, and of the speed of sound

from the hydrodynamic value c_0 to higher value c_∞, when the excitation frequency $E/\hbar$ is comparable with $1/\tau$: such a dispersion of velocity is typically observed changing the thermodynamic state of the system (T), and therefore τ.

The extension to larger Q and E values up to $Q \approx Q_m$, has been experimentally more difficult, until the development of inelastic X-ray scattering (IXS) spectroscopy with meV energy resolution. The highly developed inelastic neutron scattering (INS) technique, in fact, cannot be easily applied at Q-transfers smaller than $10\,\mathrm{nm}^{-1}$ on typical liquid systems because the required energy transfers are too large for standard INS spectrometer setups.

2. IXS with *milli*-electron-volt energy resolution

The study in condensed matter of atomic density fluctuations on the scale of inter-particle separations is, traditionally, the domain of neutron spectroscopies. The principal reason making neutrons particularly suitable for these studies is the very good matching between the phase space of thermal neutrons and that of phonon-like collective excitations. In fact, the energy of neutrons with wavelengths of the order of inter-particle distances is about 100 meV, and this value is comparable to the energies of phonons with wavelengths in the *nano*-meter range. As a consequence, one can determine $S(Q,E)$ without requiring an excessive relative energy resolution in the spectrometers, and therefore one can exploit very efficiently the intensity of the source.

In principle, also X-rays can be used to determine $S(Q,E)$. The IXS cross-section, under certain circumstances, has an expression formally very similar to that valid for neutrons, and the coupling of X-rays and neutrons to the density fluctuations is of the same order of magnitude. This can be understood by considering the existing complementarity between X-ray and neutron Bragg diffraction, and extending it to the dynamics, i.e., to the density fluctuations around the static structure. The X-ray scattering cross-section is derived considering the interaction between the electrons and the X-ray electromagnetic field. In the weak relativistic limit, the interaction Hamiltonian is composed of four terms. Two describe the diamagnetic (Thomson term) and paramagnetic (photoelectric absorption term) coupling of the photon field to the electron current. The other two, considerably smaller, describe the magnetic couplings. In the present context, we will consider only the charge scattering arising from the Thomson interaction Hamiltonian, an approximation which requires the use of an X-ray energy sufficiently far away from a photoabsorption edge of a core-line in the investigated system. The Thomson interaction Hamiltonian, $H_{\mathrm{I-Th}}$; is given by

$$H_{\mathrm{Th}} = \frac{1}{2} r_0 \sum_j A^2(\mathbf{r}_j, t). \tag{2}$$

Here $r_0 = e^2/mc^2$ is the classical electron radius, $A(\mathbf{r}_j, t)$ is the vector potential of the electromagnetic field at $\mathbf{r}_j$, co-ordinate of the jth electron. The sum extends over all the electrons in the system. The double differential cross-section is proportional to the number of incident probe photons which are scattered with an energy and momentum variation within the energy range ΔE and the solid angle $\Delta\Omega$. Considering a scattering event where a photon of energy E_i, wave vector $\mathbf{k}_\mathrm{i}$, and polarisation ε_i, is scattered into a final state of energy E_f, wave vector $\mathbf{k}_\mathrm{f}$, and polarisation ε_f, while the electrons system goes from the initial state $|I\rangle$ to the final state $|F\rangle$, the double differential cross-section is

$$\frac{\partial^2\sigma(E,\Omega)}{\partial\Omega\,\partial E} = r_0^2(\varepsilon_\mathrm{i}\cdot\varepsilon_\mathrm{f})^2 \frac{k_\mathrm{f}}{k_\mathrm{i}} \times \sum_{I,F} p_I \times |\langle I| \sum_j \mathrm{e}^{\mathrm{i}\mathbf{Q}\cdot\mathbf{r}_j} |F\rangle|^2 \times \delta(E - E_\mathrm{i} + E_\mathrm{f}), \tag{3}$$

where $\mathbf{Q} = \mathbf{k}_\mathrm{i} - \mathbf{k}_\mathrm{f}$ is the momentum transferred to the system. The sum over the initial and final states is the statistical average, and P_I corresponds to the population of the initial state. This expression can be written in terms of the correlation function of the atomic density under the following assumption: (i) The adiabatic approximation, i.e., the separation of a quantum state $|S\rangle$ of the system into the product of an electronic part, $|S_\mathrm{e}\rangle$, which

depends only parametrically from the nuclear coordinates, and a nuclear part, $|S_N\rangle$: $|S\rangle = |S_e\rangle|S_N\rangle$; when the exchanged energies that are small with respect to the excitations energies of electrons in bound core states: considering the energy of typical phonon excitations, this is indeed the case in basically any atom. Moreover, (ii) we will consider a situation in which the electronic part of the total wave function is not changed by the scattering process. By the introduction of the dynamic structure factor $S(Q,E)$ as defined in Eq. (1), the double differential cross-section for IXS from atomic density fluctuations reduces, for a monoatomic system, to the following expression:

$$\frac{\partial^2\sigma(E,\Omega)}{\partial\Omega\,\partial E} = r_0^2(\varepsilon_i\cdot\varepsilon_f)^2\frac{k_f}{k_i}|f(Q)|^2S(Q,E). \quad (4)$$

In the limit $Q\to 0$, the form factor $f(Q)$ is equal to the number of electrons localised on the scattering atom, Z. Increasing the value of Q, the form factor decays rapidly with a decay constant for each electron of the order of the inverse of its electronic shell dimension. At Q-values large with respect to these dimensions, therefore, the IXS from density fluctuations is strongly reduced.

In spite of the strong analogies between inelastic neutron and X-ray scattering cross-sections, the use of X-rays has been so far limited mainly for the following reasons:

- Photons with wavelength $\lambda = 0.1$ nm have energies of about 10 keV. Therefore, the study of phonon excitations in the meV region requires at least a relative energy resolution $\Delta E/E \approx 10^{-7}$.
- The total absorption cross-section of X-rays of 10 keV energy is limited by the photoelectric absorption process ($\propto Z^4$) and not by the Thomson scattering process ($\propto Z^2$). Consequently, the Thomson scattering channel is not very efficient for system with high Z.
- The rapid decrease of the atomic form factor with increasing Q is responsible for a drastic reduction of the scattering cross-section, already at relatively small momentum transfer values.

Despite these important limitations, however, there are situations where the use of X-rays has important advantages over neutrons. A specific case is based on the general consideration that it is not possible to study acoustic excitations propagating with a speed of sound, c, using a probe particle with a speed c_i smaller than c. This limitation is not particularly relevant in neutron spectroscopy in studies of crystalline samples. Here, the translation invariance allows to study the acoustic excitations in high-order Brillouin zones, and this overcomes the mentioned kinematics limit on phonon branches with steep dispersions. On the contrary, the situation is very different for topologically disordered systems: here, with only few exceptions and in a limited $Q-E$ region, it has not been possible to determine the dynamic structure factor using neutrons. In these systems, in fact, the absence of periodicity imposes that the acoustic excitations must be measured at small momentum transfers.

The previous arguments explain why, in the study of disordered systems, the IXS technique can be extremely valuable. Considering, in fact, that the energy transfers for the X-ray case are small compared to the incident and scattered photon energies—$E_i \approx E_f$ and $|\mathbf{k}_i| \approx |\mathbf{k}_i|$—a given scattering angle θ_s completely determines the magnitude of the momentum transfer, Q, independently of the energy transfer, E:

$$\frac{Q}{k_i} = 2\sin\left(\frac{\theta_s}{2}\right). \quad (5)$$

From this relation one sees that, for phonon-like excitations, in IXS there is no limitation in energy transfer at a given momentum transfer.

Moreover, the IXS cross-section is highly coherent, contrary to neutrons where sometimes it is necessary to separate "a posteriori" the coherent (genuine collective part), $\propto S(Q,E)$, from the incoherent (single particle), $\propto S(Q,E)$. Other remarkable advantages are related to the multiple scattering processes, in general strongly suppressed by the photoelectric absorption process, and to the possibility of having very small beam-sizes on the sample that allows to study systems available in small quantities and/or their investigation in extreme thermodynamic conditions.

The previous discussion illustrates how the IXS technique can be very useful and complementary

to INS, although by no means can be viewed as an alternative to the powerful neutron methodologies. In particular, the development of the X-ray spectroscopy provided access to an extremely important region of the $E-Q$ plane, in particular, to that of the small Q-values, where the acoustic excitations have energies which are not of easy access to neutrons [4].

The most common way to obtain a highly monochromatic X-ray beam from a white source is using a Bragg reflection from a perfect crystal. The largest resolving power, $(E/\Delta E)_{\mathbf{h}}$, obtained from the reflection $\mathbf{h}$ of an ideal crystal, is an intrinsic property of the considered crystal and can be deduced within the framework of the dynamical theory of X-ray diffraction [5]. Here $(\Delta E/E)_{\mathbf{h}}$ is proportional to the square of the effective separation between the diffracting planes $d_{\mathbf{h}}$; and to the form factor at $Q_{\mathbf{h}} = \pi/d_{\mathbf{h}}$, and is independent of the Bragg angle θ_{B}. Qualitatively, these results can be understood recalling that in crystal diffraction the penetration of the X-ray beam is finite even in absence of photoelectric absorption, as the reflectivity of the crystal planes is finite. Therefore the number of planes participating to the Bragg reflection process is also finite, and $(\Delta E/E)_{\mathbf{h}}$ is inversely proportional to their number. Increased resolving powers are obtained using reflections of increased order: this is a direct consequence of (i) the reduction of the form factor (which is the reflection coefficient for the amplitude of the electric field, see Eq. (5) for increasing Q, and of (ii) the proportionality between $(\Delta E/E)_{\mathbf{h}}$ and $d_{\mathbf{h}}^2$. In order to obtain an X-ray beam with high-resolving power, it is therefore necessary to use high-order Bragg reflections, and to have highly perfect crystals [6].

Some geometrical conditions, beside the energy resolution issues, are important to use efficiently a high-order Bragg reflection. From the differentiation of Bragg law, one obtains a contribution to the relative energy resolution due to the angular divergence $\Delta\theta$ of the beam impinging on the crystal: $\Delta E/E = \Delta\theta \cot(\theta_{\mathrm{B}})$. To reach the intrinsic energy resolution of the considered reflection, It is necessary to keep $(\Delta E/E)_{\mathbf{h}} \leqslant \Delta\theta \cot(\theta_{\mathrm{B}})$. In typical Bragg reflection geometry $\cot(\theta_{\mathrm{B}}) \approx 1$, and, for high-order reflections with $(\Delta E/E)_{\mathbf{h}} \approx 10^{-8}$, the required angular divergence should be in the 10^{-8} rad range, i.e., values much smaller than the collimation of X-ray beams available even at the new third generation synchrotron radiation sources (10^{-5} rad). This geometrical configuration would induce a dramatic reduction of the number of photons Bragg reflected from the monochromator and analyser crystals within the desired spectral bandwidth. An elegant way to overcome this problem is working in an extreme backscattering geometry, i.e., the use of Bragg angles very close to 90°. In this way, the small values of $\cot(\theta_{\mathrm{B}})$ ($\theta_{\mathrm{B}} \approx 89.98^\circ$ gives $\cot(\theta_{\mathrm{B}}) \approx 10^{-4}$) allow acceptable values of $\Delta\theta$ up to above 10^{-5} rad, and therefore they become even larger than the divergence $\approx 10^{-5}$ rad of typical synchrotron radiation from an undulator source.

Although the requirements on the energy resolution of the monochromator and of the analyser are the same, the necessary angular acceptances are very different. The X-ray beam incident on the monochromator has the angular divergence of the X-ray source, and therefore one can use a flat perfect crystal. In the case of the analyser crystal, however, the optimal angular acceptance is dictated by the desired momentum resolution. Considering values of ΔQ in the range of $0.5\,\mathrm{nm}^{-1}$ reasonable in the region of exchanged momenta of $1–10\,\mathrm{nm}^{-1}$, the corresponding angular acceptance of the analyser crystal must be ≈ 10 mrad or higher, which is again an angular range well above the acceptable values even close to backscattering geometries. A solution consists in arranging a large number of undistorted perfect flat crystals on a spherical surface. This method has been utilised in the construction of the ESRF spectrometer on BL21-ID16: namely, approximately 10,000 silicon perfect crystals of surface size $0.7 \times 0.7\,\mathrm{mm}^2$ and thickness 3 mm have been glued on a spherical substance of 6500 mm radius. This ''perfect silicon crystal with a spherical shape'' is the meV energy resolution analyser of the BL21-ID16 beamline.

In Fig. 1 we report the main optical elements of the ESRF IXS beamline. The instrument, a triple axis spectrometer, has as first axis the monochromator crystal, whose role is to determine the

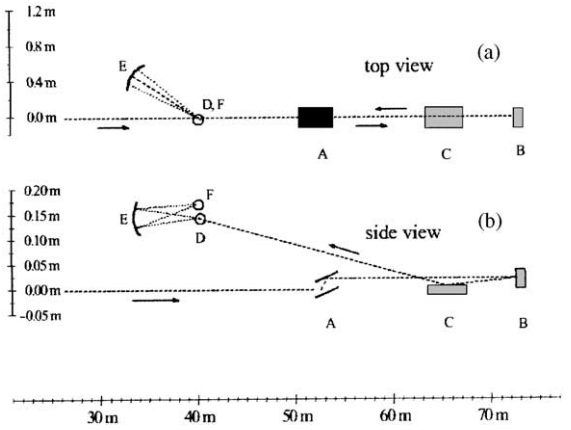

Fig. 1. Schematic layout of the IXS beamline ID16-BL21 at ESRF. The different components and their function are sketched in the figure: (A) pre-monochromator; (B) main monochromator; (C) toroidal mirror; (D) scattering centre (sample); (E) analyser crystal; (F) detector.

energy, E_i, of the incident photons. The second axis is established by the scattering sample, where one selects the scattering angle θ_s, and therefore the exchanged momentum according to Eq. (6). The third axis is provided by the analyser crystal, whose role is the determination of the energy E_f of the scattered photons. To maintain the backscattering geometry for any energy transfer, a certain energy difference between analyser and monochromator is obtained by keeping the Bragg angle constant, and by changing the temperature of the monochromator with respect to that of the analyser. This has the effect of varying the relative lattice parameter, and therefore the value of the reflected energies. Considering that $\Delta d/d = \alpha\Delta T$, with $\alpha = 2.56 \times 10^{-6}\,K^{-1}$ in silicon at room temperature, in order to obtain an energy step of about one-tenth of the energy resolution, i.e. $\Delta E/E \approx 10^{-9}$, it is necessary to control the monochromator crystal temperature with a precision of about 0.5 mK, throughout a temperature bath controlled with an active feedback system.

The X-ray beam from the undulator odd-harmonics has an angular divergence of approximately $15 \times 40\,\mu rad$ full width at half maximum (FWHM), a spectral bandwidth $\Delta E/E \approx 10^{-2}$, and an integrated power within this divergence of the order of 200 W. This beam is first pre-monochromatised to $\Delta E/E \approx 2 \times 10^{-4}$ using a Si(1 1 1) double crystal device kept in vacuum and at the cryogenic temperature of ≈ 120 K (element A in Fig. 1). The photons from the pre-monochromator reach the high-energy resolution backscattering monochromator (element B in Fig. 1). This is a flat symmetrically cut silicon crystal oriented along the (1 1 1) direction, at a temperature controlled with a precision of 0.2 mK in the 285–295 K temperature region. The Bragg angle on the monochromator is $\theta_B = 89.98^\circ$. The monochromatic beam impinges on a focusing toroidal mirror (element C in Fig. 1), which gives at the sample (element D in Fig. 1) a beam-size of 150(vertical) × 350(horizontal) μm^2 FWHM. The analyser system (element E in Fig. 1) is made of an entrance pinhole, slits in front of the analyser crystal to set the desired momentum resolution, the analyser spherical crystal in backscattering geometry ($\theta_B = 89.98^\circ$), an exit pinhole in front of the detector, and the detector itself (element F in Fig. 1). There are, in fact, five independent analyser systems with a fixed angular offset in the scattering plane among themselves. They are mounted on a 7 m long arm which can rotate around a vertical axis passing through the scattering sample. This rotation allows to determine the scattering angle θ_s for each of the five analysers, and therefore the corresponding exchanged momentum. The arm operates between 0° and 15°. The spherical analyser crystals are kept at constant temperature with a precision of 0.2 mK, and operate at the same reflection of the monochromator in Rowland circle geometry with 1:1 magnification. The detectors are inclined silicon diodes with an equivalent thickness of 2.5 mm.

The resolution performance of any of the five spectrometer channels depends on the selected Si ($h\,h\,h$) reflection of monochromator and analyser, with typical values of 1.5 meV achieved when one utilises the Si(11 11 11) reflection [7]. At this order, the angular offset between the five analysers corresponds to an exchanged momentum difference of $3\,nm^{-1}$. The instrumental response function of one of the five channels is reported in Fig. 2. This has been obtained by measuring the scattering from a disordered sample of Plexiglas at a Q-transfer corresponding to $Q = Q_m = 10\,nm^{-1}$,

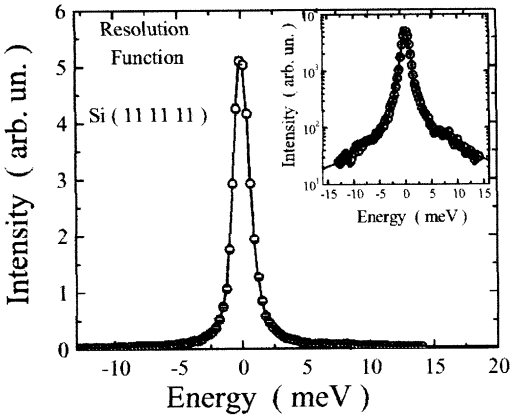

Fig. 2. Resolution function of the whole instrument obtained using the monochromator and analyser Si(11 11 11) reflections in backscattering geometry and measuring the elastic scattering from a plastic sample. The solid line is a Lorentzian fit to the data, used to determine the FWHM of the resolution function (1.5 ± 0.2 meV). In the inset the same data are reported in logarithmic scale to better appreciate the shape of the tail of the resolution function.

and at $T = 20$ K, in order to maximise the elastic contribution to the scattering.

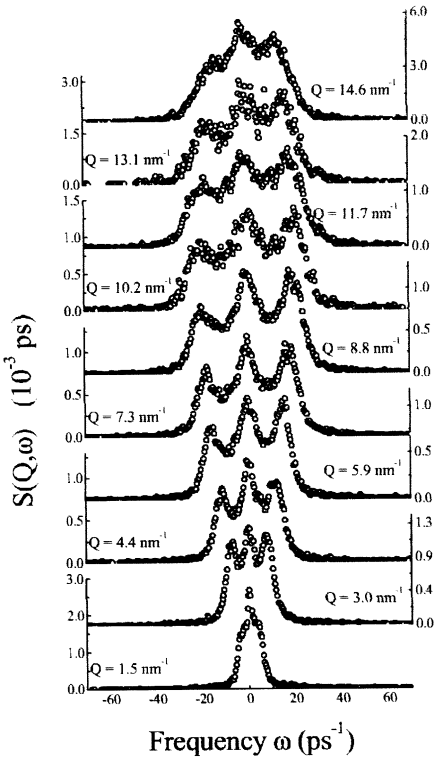

Fig. 3. Dynamic structure factor of liquid sodium measured by IXS at several fixed Q-values. Data have been normalised according to the procedure described in Ref. [4].

3. Selected examples

In this section two examples of the determination of the dynamic structure factor by IXS technique will be presented, with reference to some recent experiments devoted to the study of the high-frequency dynamics in simple liquids (sodium) and strong glasses (v-SiO_2). In Fig. 3, a selection of $S(Q,\omega)$ data at several fixed Q-values is reported for liquid sodium. Data have here been normalised to the incident monitor and then reported in absolute units by means of the lower order sum rules holding for the dynamic structure factor (see Ref. [4] for further details). As apparent, the two inelastic components (stokes and antistokes sides of the spectra) exhibit the typical dispersive behaviour of acoustic phonons observed in crystalline systems. The associated sound velocity is defined [1] as the ratio between the peak position $\omega_l(Q)$ of the current correlation function $J(Q,\omega) = \omega^2/Q^2 S(Q,\omega)$ and the transferred momentum Q. In Fig. 4 we report both the peak position and speed of sound (inset) as function of Q. As can be noticed, in the IXS characteristic Q-region, say 1–10 nm^{-1}, the value of the sound speed exceeds the value expected in the $Q \to 0$ limit by about 20%. This behaviour, referred to as *positive dispersion*, is the typical signature of one or more relaxation processes active in the system. Although the details of the physics underlying this processes can be rather complex and too far from the purpose of this paper, the basic mechanisms leading to such a phenomenon can be easily catched. In an IXS/INS experiment, one normally probes the behaviour of a fourier component of the spontaneous density fluctuation of the system, selected by imposing a defined value of exchanged momentum and energy. In a non-crystalline system, such Fourier components (i.e., sinusoidal density patterns) are

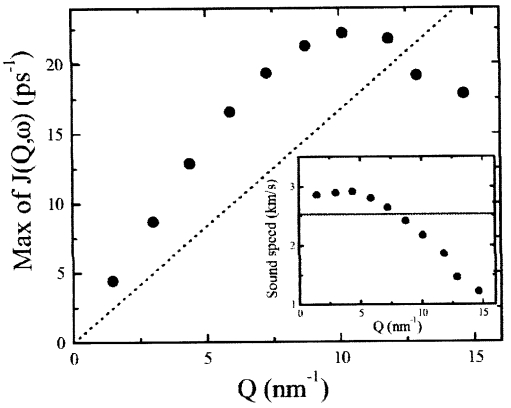

Fig. 4. Main plot: dispersion curve $\omega_l(Q)$ (full dots ●) of liquid sodium compared to the low-frequency, isothermal, behaviour (dotted line). Inset: speed of sound in the same notation of the inset.

not stationary states, so that they are expected to relax evolving towards the stationary state corresponding to a certain thermodynamic state. This tendency to relax strongly depends on the characteristic frequency of the considered density fluctuation. In particular, in the low-frequency limit the system *has time* to relax and the acoustic modes will be damped by viscous effects. On the contrary, in the high-frequency limit the density fluctuation dynamics occurs over a so short timescale that the system *has no time* to rearrange its atomic/molecular position and consequently it will exhibit an elastic response. The acoustic properties associated to the two different regimes are obviously much different. In particular, the speed of sound is expected to be higher in the elastic limit (solid-like response) than in the viscous limit (liquid-like response). Now in several systems, around the melting temperature, the transition between these two different regime always occurs in the *Thz* region, that is the one typically accessed probing the characteristic wavelengths of IXS.

In Fig. 5 we report the result of a similar experiment performed on a vitreous silica sample, customarily considered as the prototype of the strong glasses. In this case one clearly observes the presence of a much larger elastic line that tends to hide the acoustic mode. Such elastic contribution, in the frequency range typically probed by IXS, is

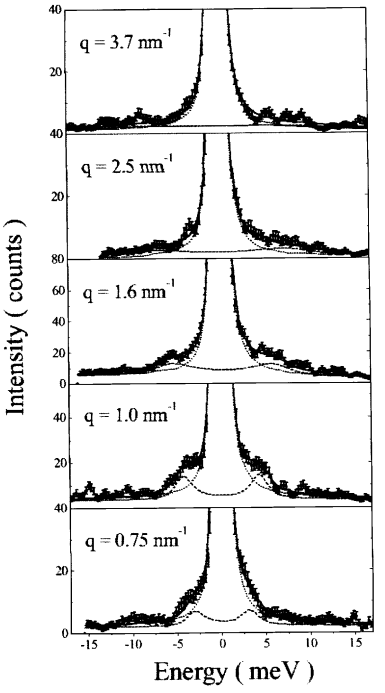

Fig. 5. Dynamic structure factor of vitreous silica at $T = 1350$ K measured by IXS at several fixed Q-values. Intensity is here reported in arbitrary units due to the strong elastic signal that prevents a normalisation accurate as in the case of liquid metals. Dotted and dashed lines indicate the resolution and the inelastic (DHO) contribution, respectively.

a measure of the relaxation time of the system. During the glass formation, a structural arrest takes place around the glass formation temperature, $T-g$, where the value of the relaxation time increases abruptly by several orders of magnitude. This explains the marked difference in the central peak of the $S(Q,\omega)$ of a liquid and a glass. On the other side, the inelastic features show a similar behaviour: even in vitreous silica acoustic modes exist and propagate with a characteristic speed of sound, as shown in Fig. 6. Due to the smallness of this contribution compared to the resolution tails, information on the acoustic properties can here only be extracted throughout a fitting procedure introducing a model function, in this case a damped harmonic oscillator (DHO) lineshape [8]. In this case the sound speed almost coincides with the adiabatic one, as the relaxation time is so long that all over the probed Q-range the system

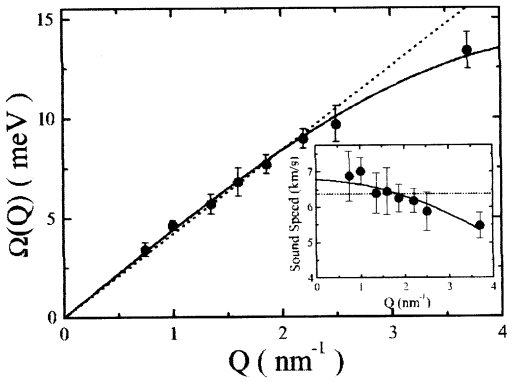

Fig. 6. Main plot: dispersion curve $\omega_l(Q)$ (full dots ●) of vitreous silica compared to the low-frequency, isothermal, behaviour (dotted line …). Inset: speed of sound in the same notation of the inset.

response is elastic. It is worth to mention that, recently, experimental deviations from this over-simplified picture have been investigated, since the presence of a very fast relaxation mechanism has been found in numerical studies of monoatomic glasses [9].

References

[1] U. Balucani, M. Zoppi, Dynamics of the Liquid State, Oxford Science Publishers, Oxford, 1994.

[2] W.E. Alley, B.J. Alder, S. Yip, Phys. Rev. A 27 (1983) 3174; C. Bruin, J.P.J. Michels, J.C. Van Rijs, L.A. de Graaf, I.M. deSchepper, Phys. Lett. 110A (1985) 40.

[3] I.M. de Schepper, J.C. Van Rijs, A.A. van Well, P. Verkerk, L.A. de Graaf, Phys. Rev. A 29 (1984) 1602;
U. Bafile, F. Barocchi, M. Neumann, P. Verkerk, J. Phys. Condens. Matter 6 (1994) A107.

[4] F. Sette, G. Ruocco, M. Krisch, U. Bergmann, C. Masciovecchio, V. Mazzacurati, G. Signorelli, R. Verbeni, Phys. Rev. Lett. 75 (1995) 850;
G. Ruocco, F. Sette, M. Krisch, U. Bergmann, C. Masciovecchio, V. Mazzacurati, G. Signorelli, R. Verbeni, Nature 379 (1996) 521;
F. Sette, G. Ruocco, M. Krisch, C. Masciovecchio, R. Verbeni, U. Bergmann, Phys. Rev. Lett. 77 (1996) 83;
T. Scopigno, U. Balucani, A. Cunsolo, C. Masciovecchio, G. Ruocco, F. Sette, R. Verbeni, Europhys. Lett. 50 (2000) 189;
T. Scopigno, U. Balucani, G. Ruocco, F. Sette, Phys. Rev. Lett. 85, 4076;
T. Scopigno, U. Balucani, G. Ruocco, F. Sette, J. Phys. C 12 (2000) 8009;
T. Scopigno, U. Balucani, G. Ruocco, F. Sette, Phys. Rev. E 63 (2001) 011210.

[5] H. Zachariasen, Theory of X-ray Diffraction in Crystals, Dover, New York, 1944.

[6] R. Verbeni, F. Sette, M.H. Krisch, U. Bergmann, B. Gorges, C. Halcoussis, K. Martel, C. Masciovecchio, G. Ruocco, H. Sinn, J. Synch. Radiat. 3 (1996) 62.

[7] C. Masciovecchio, U. Bergmann, M.H. Krisch, G. Ruocco, F. Sette, R. Verbeni, Nucl. Instrum. Methods B-111 (1996) 181;
C. Masciovecchio, U. Bergmann, M.H. Krisch, G. Ruocco, F. Sette, R. Verbeni, Nucl. Instrum. Methods B-117 (1996) 339.

[8] B. Fak, B. Dorner, Institute Laue Langevin, Technical report No. 92FA008S, 1992, Grenoble, France.

[9] G. Ruocco, F. Sette, R. Di Leonardo, G. Monaco, M. Sarnpoli, T. Scopigno, G. Viliani, Phys. Rev. Lett. 84 (2000) 5788.